Radio Science, Volume 33, Number 3, Pages 517–533, May–June 1998

Interpretation of angle-of-arrival measurements in the lower atmosphere using spaced antenna radar systems

Jorge L. Chau and Ben B. Balsley

Cooperative Institute for Research in Environmetal Sciences, University of Colorado, Boulder

Abstract. On the basis of scattering theory, we present four different contributions to angle-of-arrival (AOA) measurements using spaced antenna (SA) radar systems. We show that the measurement of the scattering parameters is needed to estimate most AOA contributions (e.g., tilt angle of layers). We analyze a general SA system (i.e., receiving antennas not necessarily symmetrically placed about the transmitter) and show, theoretically, that such systems can be used for vertical velocity corrections without explicitly knowing the scattering parameters (e.g., correlation lengths). The theoretical AOA expressions are compared with lower atmospheric data (3-21 km) obtained with the Jicamarca VHF radar system in Perú. We compare the AOAs obtained by a time and a frequency domain method, giving both methods essentially the same information. While the results are comparable, frequency domain AOAs tend to exhibit more "outliers." From examination of time series of these AOA measurements, we find some short, but predominantly long-period oscillations (>12 hours) with amplitudes of ~1°.

1. Introduction

Atmospheric measurements by very high frequency (VHF) radars tend to show aspect sensitivity effects, i.e., the received signal strength decreases as the beam is tilted off vertical [e.g., *Green and Gage*, 1980; *Röttger and Liu*, 1978; *Tsuda et al.*, 1986, 1997b]. Usually, the aspect sensitivity function is centered at zenith. Some observations, however, show that on occasions the highest reflectivity arrives from small off-vertical locations (<2°) [*Green and Gage*, 1980; *Röttger and Ierkic*, 1985; *Röttger et al.*, 1990; *Tsuda et al.*, 1997a]. These off-vertical centers have been related to tilted scattering/reflecting structures [e.g., *Larsen and Röttger*, 1991; *Palmer et al.*, 1991; *Röttger et al.*, 1990]. *Tsuda et al.* [1997a] recently suggested that these off-vertical centers are caused by a corrugated layer that is modified following the vertical displacement caused by gravity waves.

Measurements of these off-vertical centers require systems with sufficient flexibility in beam-pointing and beam-steering capabilities, like the MU radar in Japan [see *Fukao et al.*, 1990], or, alternatively, a spaced antenna (SA) system [*Hocking et al.*, 1989; *Larsen and Röttger*, 1989].

Most VHF radars currently operate in a Doppler beam swinging (DBS) mode, where the antenna beam is sequentially switched through a series of beam position (at most five). Because of the lack of many, closely spaced, beam positions, measurements of off-vertical centers are not performed with these radars. SA systems, on the other hand, are able of obtaining angle-of-arrival (AOA) returns by measuring the phase path differences between signal returns using three or more spatially separated, vertically pointing, receiving antennas [*Röttger and Ierkic*, 1985]. These AOA measurements can be associated with a mean off-vertical signal return when uniform scattering volume is assumed [e.g., *Liu et al.*, 1990]. On the other hand, if discrete point-like scatterers are assumed, the AOAs at different Doppler frequencies (Doppler sorting) can be used to identify such scatterers [e.g., *Adams et al.*, 1986; *Franke et al.*, 1990; *Palmer et al.*, 1995]. In this work we are assuming a statistically homogeneous scattering medium.

AOA measurements at VHF have been used to correct vertical wind measurements by correcting for "leakage" of the horizontal wind into the vertical measurements when off-vertical returns are present

Paper number 98RS00749.
0048-6604/98/98RS-00749$11.00

[*Larsen and Röttger*, 1991; *Palmer et al.*, 1991; *Van Baelen et al.*, 1991]. Recently, *Vandepeer and Reid* [1995] and *Thorsen et al.* [1997] have used AOAs to measure the three-dimensional wind field using medium-frequency (MF) radars.

The importance of the relative positions of the transmitting and receiving antennas in AOA measurements and vertical velocity corrections has been pointed out by *May* [1993]. May also suggested that these measurement should be done with SA systems using "collocated" transmitting and receiving antennas in order to unambiguously interpret the AOA in terms of tilted layers. In addition, according to May, the leakage of the horizontal velocity in the vertical beam can be accurately removed only if the antennas are collocated (i.e., receiving antennas are symmetrically placed about the transmitter).

In this paper we present the theoretical aspects of various contributions to AOA measurements using SA systems. This development will help to clarify the interpretation of AOA measurements and their usage in vertical velocity corrections. We have expanded on the scattering model presented by *Doviak et al.* [1996] (hereinafter referred to as Doviak et al.) to investigate AOA returns. Briefly, Doviak et al.'s development (p. 157) "ties the properties of a turbulently advected scattering medium to the cross correlation and cross spectrum of signals in a general configuration of receiving and transmitting antennas." A similar scattering model has been presented by *Liu et al.* [1990]; however, this latter derivation has the constraints that the SA system has to be collocated and the receiving and transmitting antennas are assumed to be of equal sizes.

Our modifications to Doviak et al.'s work consist of adding a tilted layer and a slightly off-vertical transmitting (or receiving) beam and of explicitly showing the phase terms of Doviak et al.'s original model. We then examine two different methods (time and frequency domain) for determining AOAs. We also analyze an expression for the statistical errors in these measurements. AOA measurements using noncollocated SA systems are discussed in section 3 in terms of vertical velocity corrections and off-vertical atmospheric returns. In section 4, we compare AOA results obtained from both time and frequency domain methods. In section 4 we also compare some of the expressions developed in section 2 against experimental data. In addition, a number of interesting time series of orthogonal AOA results are shown. A summary of our results is provided in section 5.

2. Angle-of-Arrival Theory for SA Systems

In this section, assuming horizontally isotropic scattering, we first use the scattering theory presented by Doviak et al. to show different contributions to AOA measurements. We then present two different methods of measuring AOAs. Finally, we relate a previously published statistical error for AOA measurements [*Thorsen*, 1996] with Doviak et al.'s development. Expressions for the horizontal anisotropic case are derived in the appendix, and the results are related to the horizontal isotropic case in this section.

2.1. AOA Contributions

Here we make use of the formulation derived by Doviak et al. by including some additional off-vertical contributions and by explicitly presenting the important phase terms of the complex cross-correlation functions (CCFs). As pointed out by *Röttger and Ierkic* [1985], AOAs are obtained from the phase differences between signal returns at receiving antennas. These phase differences can be obtained from the phase terms of the complex CCFs. The end result will be a modified expression of the phase term of the normalized CCF given by Doviak et al.'s equation (58),

$$\phi_{ij}(\tau) = -2k_0 v_{0z}\tau \tag{1}$$

where ϕ_{ij} is the phase term of the CCF between receiving antennas i and j, k_0 is the radar wave number, v_{0z} is the vertical velocity, and τ is a time delay. It is important to point out that (58) of Doviak et al. is valid for collocated SA systems and is a simplify version of their (56). We consider the following AOA contributions.

2.1.1. Tilted layer contribution. We have represented a tilted layer effect by incorporating a tilted spatial spectrum of the refractive index field. This tilted spectrum is represented by the following Gaussian function:

$$\Phi_n(\boldsymbol{K}) = \Phi_n(0)\exp\left[-\frac{\tilde{\rho}_{ch}^2\,|\boldsymbol{K}_h - K_z\boldsymbol{\delta}_0|^2}{2}\right] \exp\left[-\frac{\rho_{cz}^2\,|\boldsymbol{K}_h|^2 + \rho_{cz}^2 K_z^2}{2}\right] \tag{2}$$

where

$$\tilde{\rho}_{ch}^2 = \rho_{ch}^2 - \rho_{cz}^2 \tag{3}$$

$$\boldsymbol{\delta}_0 = (\delta_{0x}, \delta_{0y}) \tag{4}$$

ρ_{ch} and ρ_{cz} are the irregularity correlation lengths in the parallel and orthogonal directions of the tilted layer (see Figure 1), and δ_{0x} and δ_{0y} are the small (to a first-order approximation) off-vertical angles of the normal to the tilted plane in the x and y axes, respectively. Note that if $\delta_0 = (0,0)$, equation (2) is equal to Doviak et al.'s (28) and similar to *Liu et al.* [1990, equation (13)].

Using our (2) in Doviak et al.'s (21) and assuming that $\Phi_n(K)$ varies slowly compared with the spectral sampling function $[F_s(K)]$ for K along K_z about the Bragg wavenumber $(2k_0)$, (1) becomes

$$\begin{aligned}\phi_{ij}(\tau) &\approx -2k_0 v_{0z}\tau - 4k_0[v_{0h}\cdot\Omega]\xi_h^{-2}\tau \\ &\quad +2k_0[\Delta\rho_{ij}\cdot\Omega]\xi_h^{-2} \end{aligned} \tag{5}$$

where brackets denote an inner product operation, v_{0h} is the horizontal vector velocity (v_{0x}, v_{0y}), and

$$\Omega = 2\tilde{\rho}_{ch}^2\delta_0 \tag{6}$$

$$\xi_h^2 = 2a_h^{-2} + (2\rho_{ch})^2 \tag{7}$$

$$a_h \approx k_0\alpha\sigma_T/z_0 \tag{8}$$

$$\alpha^2 = \frac{2\sigma_R^2}{\sigma_T^2+\sigma_R^2} \tag{9}$$

$$\Delta\rho_{ij} = \rho_j - \rho_i \tag{10}$$

The parameter α is a function of the difference in the sizes of the transmitting and receiving antennas, ξ_h is the horizontal correlation length of the diffraction pattern, a_h is an antenna parameter, z_0 represents the height range under study, $\sigma_{T/R}$ is the transmitting/receiving antenna beam width, and ρ_i/ρ_j is the vector position of receiving antenna i/j. The term $2\Omega\xi_h^{-2}$ is similar to the anisotropic part of *Muschinski* [1996, equation (6)]. Moreover, this term is proportional to the antenna beam width when the antenna beam width is less than the width of $\Phi_n(K)$. The width of $\Phi_n(K)$ is $\propto 1/\rho_{ch}$ and is also proportional to aspect sensitivity width (θ_s) used by *Holdsworth and Reid* [1995].

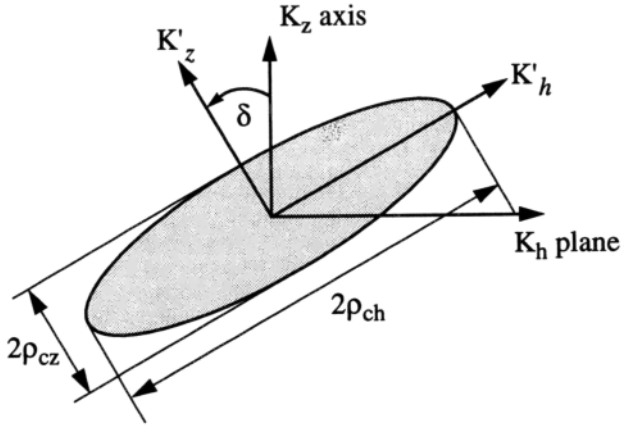

Figure 1. A cross section of a tilted correlation ellipsoid for a horizontally isotropic scatter.

This off-vertical contribution could be caused by scattering/reflecting structures [*Palmer et al.*, 1998; *Röttger et al.*, 1990] that could be associated with Kelvin-Helmholtz instabilities [*Muschinski*, 1996]. Examining (5), we see that if the scatter is isotropic (i.e., $\rho_{ch} \ll a_h^{-1}$ so $\xi_h^2 \approx 2a_h^{-2}$), then there is no tilted layer contribution ($\Omega = 0$). For nonisotropic scatter, on the other hand, measurements of ξ_h^2 are needed for accurate measurements of δ_0.

2.1.2. Off-vertical beam. We now add the contribution arising from an off-vertical transmitting beam by assuming that its gain function is represented by

$$g_T^{1/2}(\rho) = g_T^{1/2}(0)\exp\left[-\frac{|\rho - z_0\theta_0|^2}{4\sigma_T^2}\right] \tag{11}$$

where ρ represents the horizontal vector (x,y), σ_T is the transmitting antenna beam width, and $\theta_0 = (\theta_{0x}, \theta_{0y})$ are the small off-vertical pointing angles in the x and y axes, respectively. It is important to point out that the transmitter is located at (0,0) coordinates in the x-y plane and that this modification does not change the Fresnel zone centers. In addition, we have assumed a nontilted spatial spectrum of the refractive index field.

Using our (11) in Doviak et al.'s (10), equation (1) is now modified and represented by

$$\begin{aligned}\phi_{ij}(\tau) &\approx -2k_0 v_{0z}\tau - 4k_0[v_{0h}\cdot\Psi]\xi_h^{-2}\tau \\ &\quad +2k_0[\Delta\rho_{ij}\cdot\Psi]\xi_h^{-2} \end{aligned} \tag{12}$$

where

$$\Psi \approx \frac{\alpha^2\theta_0}{2a_h^2} \tag{13}$$

In (12), note the dependence on ρ_{ch} via ξ_h^2. For a horizontally isotropic atmosphere, i.e., $\xi_h^2 \approx 2a_h^{-2}$, this contribution will depend just on the pointing direction of the antennas, the antenna beam widths, and the height range. If the antennas are identical and the receiving antennas are symmetrically located about the transmitter, then (12) is similar to the phase term of *Pan and Liu* [1992, equation (12)].

In the case the receiving beams are pointing off vertical, instead of the transmitting beam, Ψ is given by

$$\Psi \approx \frac{\alpha^2 \sigma_T^2 \theta_0}{2\sigma_R^2 a_h^2} \tag{14}$$

where we have assumed the following function for the receiving beam:

$$g_R^{1/2}(\rho) = g_R^{1/2}(0) \exp\left[-\frac{|\rho - (\rho_i - z_0\theta_0)|^2}{4\sigma_R^2}\right] \tag{15}$$

Off-vertical pointing beams could be due to small imperfections on vertically directed antennas [*Huaman and Balsley*, 1996] or to intentional tilting of the antenna beams. For example, *Vandepeer and Reid* [1995] used off-vertical beam directions (10°) in their SA configuration to obtain the wind vector from AOA measurements.

2.1.3. Geometrical contribution dependent on ρ_{ch}. For this third contribution, we have again assumed a nontilted spatial spectrum of the refractive index field. By grouping the geometrical phase terms that depends on ρ_{ch} (1) is modified into

$$\begin{aligned}\phi_{ij}(\tau) \approx\ & -2k_0 v_{0z}\tau - 4k_0[\boldsymbol{v}_{0h} \cdot \boldsymbol{\Gamma}_{ij}]\xi_h^{-2}\tau \\ & +2k_0[\Delta\boldsymbol{\rho}_{ij} \cdot \boldsymbol{\Gamma}_{ij}]\xi_h^{-2}\end{aligned} \tag{16}$$

where

$$\boldsymbol{\Gamma}_{ij} \approx -\frac{(\boldsymbol{\rho}_i + \boldsymbol{\rho}_j)(\alpha^2 - 1)}{4z_0 a_h^2} \tag{17}$$

Examining (17), $\boldsymbol{\Gamma}$ is a function of the geometry of the system, i.e., of the antenna positions and of the antennas sizes (α), and decreases with increasing height range. However, this geometrical contribution varies as ρ_{ch} changes (via ξ_h^2 in (16)). For example, independent of the value of ρ_{ch}, this geometric contribution becomes zero (1) when the receiving antennas i and j are located symmetrically with respect to the transmitting antenna ($\boldsymbol{\rho}_i = -\boldsymbol{\rho}_j$), or (2) when all the antennas have the same size, i.e., the same beam widths ($\alpha = 1$). Note that for an autocorrelation function ($i = j$) and if $v_{0z} = 0$, $\partial\phi_{ii}(\tau)/\partial\tau$ reduces to (36) of Doviak et al.

2.1.4. Geometrical contribution independent of ρ_{ch}. This last contribution comes from the phase terms that do not depend on ρ_{ch}. Moreover, the contribution of these phase terms is constant for a specific system's geometry and for a specific height. Including these geometrical phase terms, (1) becomes

$$\phi_{ij}(\tau) \approx -2k_0 v_{0z}\tau + k_0|\Delta\boldsymbol{\rho}_{ij}|\Lambda_{ij} \tag{18}$$

where

$$\begin{aligned}\Lambda_{ij} &\approx -\frac{2(D_j - D_i)}{|\Delta\boldsymbol{\rho}_{ij}|} \\ D_i^2 &= z_0^2 + |\boldsymbol{\rho}_i/2|^2 \\ D_j^2 &= z_0^2 + |\boldsymbol{\rho}_j/2|^2\end{aligned}$$

This geometrical contribution becomes zero in SA systems where the receiving antennas are equidistant from the transmitter ($|\boldsymbol{\rho}_i| = |\boldsymbol{\rho}_j|$), independent of ρ_{ch} or the pointing direction of the antennas.

It is important to mention that these four AOA contributions do not affect the magnitude of the normalized CCFs. In addition, the two geometric terms are present in Doviak et al.'s (56), although they are not shown explicitly. Moreover, the expressions just presented are valid under the condition $|\boldsymbol{\rho}_i|, |\boldsymbol{\rho}_j| \leq \sigma_T$.

Putting together all the aforementioned contributions, the phase term of the complex CCF, $c_{ij}(\tau)$, is

$$\begin{aligned}\phi_{ij}(\tau) \approx\ & -2k_0 v_{0z}\tau - 2k_0[\boldsymbol{v}_{0h} \cdot \boldsymbol{\Theta}_{ij}]\tau \\ & +k_0[\Delta\boldsymbol{\rho}_{ij} \cdot \boldsymbol{\Theta}_{ij}] + k_0|\Delta\boldsymbol{\rho}_{ij}|\Lambda_{ij}\end{aligned} \tag{19}$$

where

$$\boldsymbol{\Theta}_{ij} = 2(\boldsymbol{\Omega} + \boldsymbol{\Psi} + \boldsymbol{\Gamma}_{ij})\xi_h^{-2} \tag{20}$$

so $\boldsymbol{\Theta}_{ij}$ is an AOA that includes the tilted layer contribution, the off-vertical beam direction, one geometrical contribution, and the horizontal correlation length of the scatterers (via ξ_h^2).

We have derived this phase expression assuming horizontally isotropic scattering (i.e., $\rho_{ch} = \rho_{cx} = \rho_{cy}$). It is worthwhile to note that a similar expression can be obtained if we assume horizontally anisotropic scattering (see equation (A5)). In both scattering cases, measurements of the scattering parameters are needed to estimate most AOA contributions. The scattering parameters can be calculated from a full correlation analysis (FCA) [*Briggs*, 1984; *Holloway et al.*, 1997; *Meek*, 1980].

The need for correction of vertical velocities for horizontal leakage can be seen by examining (19). Moreover, the three-dimensional velocity vector can be obtained from this equation. This approach has been used by *Vandepeer and Reid* [1995] and *Thorsen et al.* [1997] and is called time domain interferometry (TDI).

In this derivation, we have assumed that the phase difference among receiver lines is zero. Usually, these

phase differences are not zero (e.g., different cable lengths), and calibration procedures, like the one described in section 4, are needed to removed them. Other calibration procedures have been described by *Palmer et al.* [1996], *Röttger et al.* [1990], *Thorsen et al.* [1997], and *Vandepeer and Reid* [1995].

2.2. Methods of Estimating AOAs

Basically, there are two methods to estimate AOA returns: a time domain and a frequency domain method. A description of these two methods follows.

2.2.1. Time domain method. This method was first proposed by *Röttger and Ierkic* [1985]. Basically, AOA measurements are obtained by measuring the phase angles of the CCFs at $\tau = 0$ for at least two antenna baselines. From (19), the phase of baseline $i - j$ at $\tau = 0$ is

$$\phi_{ij}(0) \approx k_0[\Delta\boldsymbol{\rho}_{ij} \cdot \boldsymbol{\Theta}_{ij}] + k_0|\Delta\boldsymbol{\rho}_{ij}|\Lambda_{ij} \qquad (21)$$

Then measuring the phase of another baseline at $\tau = 0$, knowing the positions vectors (e.g., $\boldsymbol{\rho}_1$, $\boldsymbol{\rho}_2$, and $\boldsymbol{\rho}_3$), and calculating the constant geometric terms (for instance, Λ_{12}, Λ_{13}, and Λ_{23}, for a three-receiver SA system), we can calculate the two-dimensional AOA $\boldsymbol{\Theta}$.

2.2.2. Frequency domain method. This method was discussed by *Briggs and Vincent* [1992] for the two-dimensional case. *Holdsworth* [1997] presented an extension for the three-dimensional situation. Basically, Fourier transforming Doviak et al.'s (58) and including (19), the phase of the resulting cross-spectrum function (CSF) is given by

$$\begin{aligned}\phi_{ij}(f) &= m_{ij}(f - f_{dij}) \\ &\quad + k_0[\Delta\boldsymbol{\rho}_{ij} \cdot \boldsymbol{\Theta}_{ij}] + k_0|\Delta\boldsymbol{\rho}_{ij}|\Lambda_{ij} \qquad (22)\end{aligned}$$

where

$$f_{dij} = -\frac{2}{\lambda}(v_{0z} + [\boldsymbol{v}_{0h} \cdot \boldsymbol{\Theta}_{ij}]) \qquad (23)$$

is the Doppler shift, λ is the radar's wavelength, and m_{ij} is a slope that depends on $\boldsymbol{v}_{0h}$, ξ_h^2, $\Delta\boldsymbol{\rho}_{ij}$ and the turbulence intensity (σ_t). From (22), the two-dimensional AOA $\boldsymbol{\Theta}$ can be obtained by evaluating the phase $\phi(f)$ at the frequencies $f = f_d$ and by calculating the geometrical terms Λ for at least two antenna baselines.

2.3. Statistical Errors in Time-Domain AOA Measurements

Thorsen [1996] presented an expression for the variance of the estimate of the CCF phase ϕ, assuming the following CCF:

$$\begin{aligned}C_{ij}[\tau] &= S_{ij}\exp(-8[\pi\sigma_v T_s(\tau - \tau_{pij})/\lambda]^2) \\ &\quad \exp(j\omega_d\tau T_s + \varphi_{ij}) + N_{ij}\delta[\tau] \qquad (24)\end{aligned}$$

where σ_v is the spectral width, T_s is the sampling time, τ_{pij} is the delay to the peak of C_{ij}, ω_d is a Doppler shift, φ_{ij} a phase difference, S_{ij} is the signal power, and N_{ij} is the noise power. The phase difference φ_{ij} and the delay to the peak τ_{pij} are equal to zero for $i = j$. The separate receiver noises are assumed uncorrelated ($N_{ij} = 0$ for $i \neq j$).

Instead of using (24), we have used Doviak et al.'s (58) along with (19). Then, the CCF is given by

$$\begin{aligned}C_{ij}[\tau] &= S_i S_j A_{ij}\exp\left[-\frac{(\tau - \tau_{pij}/T_s)^2}{2(\tau_c/T_s)^2}\right] \\ &\quad \exp(j\phi_{ij}[\tau]) + N_{ij}\delta[\tau] \qquad (25)\end{aligned}$$

where

$$\begin{aligned}\tau_c^2 &= \frac{1}{2[2\xi_h^{-2}\,|\boldsymbol{v}_{0h}|^2 + (2k_0\sigma_t)^2]} \\ \tau_{pij}^2 &= 2\xi_h^{-2}(\boldsymbol{v}_{0h} \cdot \Delta\boldsymbol{\rho}_{ij})\tau_c^2 \\ A_{ij} &= \exp\left(-\frac{|\Delta\boldsymbol{\rho}_{ij}|^2}{2\xi_h^2} + \frac{\tau_{pij}^2}{2\tau_c^2}\right)\end{aligned}$$

Examination of (24) and (25) shows that they are very similar. However, (25) relates its amplitude (A_{ij}), delay to the peak and correlation time (τ_c), to the SA parameters (antenna positions, antenna beam widths, etc.), and to the atmospheric parameters (horizontal velocity, turbulence intensity, and ρ_{ch}).

Using (25) and following the derivation of *Thorsen* [1996], the variance of an estimated phase is

$$\begin{aligned}E[(\delta\hat{\phi}_{ij}[\tau])^2] \approx \Bigg\{&\left(\frac{N_i^2}{S_i^2} + \frac{N_j^2}{S_j^2} + \frac{N_i^2}{S_i^2}\frac{N_j^2}{S_j^2}\right) \\ &+ \frac{\sqrt{\pi}\tau_c}{T_s}(1 - \mathrm{coh}_{ij}^2[\tau])\Bigg\}\frac{1}{2M\mathrm{coh}_{ij}^2[\tau]} \qquad (26)\end{aligned}$$

for $i \neq j$, where

$$\mathrm{coh}_{ij}^2[\tau] = A_{ij}^2\exp\left[-\frac{(\tau - \tau_{pij}/T_s)^2}{(\tau_c/T_s)^2}\right] \qquad (27)$$

$\delta\hat{\phi}_{ij} = \hat{\phi}_{ij} - \phi_{ij}$, $\hat{\phi}_{ij}$ are the measured values, ϕ_{ij} represent the true values, and M represents the number of points used in the estimate. For small τ, $E[\hat{\phi}_{ij}] = E[\phi_{ij}]$ [*Thorsen*, 1996], and therefore $E[\delta\hat{\phi}_{ij}] = 0$.

For the time domain method, the variance of the estimated phase (statistical error), is obtained by evaluating (27) at $\tau = 0$. At high signal-to-noise ratio ($\mathrm{SNR}_i = S_i^2/N_i^2$), this variance becomes

$$\varepsilon_{\phi ij}^2 = E[(\delta\hat{\phi}_{ij}[0])^2] \approx \frac{1}{2M}\frac{(1-\mathrm{coh}_{ij}^2[0])}{\mathrm{coh}_{ij}^2[0]}\frac{\sqrt{\pi}\tau_c}{T_s} \tag{28}$$

where $\mathrm{coh}_{ij}^2[0] = \exp[-|\Delta\rho_{ij}|^2/(2\xi_h^2)]$. Note that this derivation is valid for horizontally isotropic scattering. In the case of horizontal anisotropy, i.e., $\rho_{cx} \neq \rho_{cy}$, (28) remains the same. However, the coherence value $\mathrm{coh}_{ij}[0]$, is given by (A10), and the new correlation time is given by *Holloway et al.* [1997, equation (28)]. In practice, $\mathrm{coh}_{ij}^2[0]$ is calculated after the "spike" at zero lag, i.e., the noise contribution, has been removed from autocorrelation and cross-correlation functions [*Briggs*, 1984].

3. On the Use of Noncollocated SA Systems for AOA Measurements

In a collocated SA system, the geometrical center of the transmitting antenna coincides with the geometrical center of the array of receiving antennas. Examples of these systems are equilateral triangles and square configurations, where the transmitting antenna is located in the center of such configurations. In a noncollocated SA system, such geometrical centers do not coincide. In this section, we examine some issues on the AOAs obtained by noncollocated SA systems.

Examining (19), one sees that the only terms that contribute to the measured AOA and depend on the antenna positions are the geometrical terms Γ and Λ. A similar contribution has been pointed out by *Vincent et al.* [1987] and *May* [1993] (hereinafter referred to as May). On the basis of this contribution, May suggested that collocated transmitting and receiving antennas should be used in atmospheric AOA and unbiased vertical velocity measurements. In the following paragraphs we analyze these assertions.

To begin, we examine a similar example to the one given by May. A narrow transmitting beam and wide receiving beams are assumed, implying $\alpha^2 = 2$. An isotropic scatter is represented by $\xi_h^2 \approx 2a_h^{-2}$, and a specular scatter is represented by $\xi_h^2 \to \infty$. The positions of the receivers, with respect to the transmitter position, are $\boldsymbol{\rho}_1 = (2x_1, 0)$ and $\boldsymbol{\rho}_2 = (2x_2, 0)$. We assume zero vertical velocity ($v_{0z} = 0$), perfect vertically directed antennas [$\boldsymbol{\theta}_0 = (0,0)$], and atmospheric contribution centered at zenith [$\boldsymbol{\delta}_0 = (0,0)$]. With these assumptions we analyze the following two effects:

The first effect is horizontal leakage. The leakage of the horizontal velocity in the radial velocity can be seen by using (19) and evaluating the Doppler shift $d\phi_{11}(\tau)/d\tau$. The results for the isotropic and specular cases are

$$\frac{d\phi_{11}(\tau)}{d\tau} = \begin{cases} \frac{k_0(2x_1)v_{0x}}{z_0} & \text{isotropic} \\ 0 & \text{specular} \end{cases} \tag{29}$$

which are the same to those presented by May.

The second effect is receiver separation. Evaluating (19) at $\tau = 0$, the phase term $\phi_{12}(0)$ becomes

$$\phi_{12}(0) = \begin{cases} \frac{2k_0(x_1^2-x_2^2)}{z_0} & \text{isotropic} \\ \frac{k_0(x_1^2-x_2^2)}{z_0} & \text{specular} \end{cases} \tag{30}$$

where we have used a Taylor series expansion for D_1 and D_2. Again, these expressions are the same to those presented by May.

Evaluating the Doppler shift from

$$f_d = \left[\frac{d\phi_{11}(\tau)}{d\tau} + \frac{d\phi_{22}(\tau)}{d\tau}\right] \Big/ 2 \tag{31}$$

shows that the leakage of the horizontal velocity can be removed using the cross-correlation phase $[\phi_{12}(0) - k_0|\Delta\rho_{ij}|\Lambda_{ij}]$, without knowing ρ_{ch} (recall that Λ_{ij} are constant for a given height and depend just on the receiver spacing).

On the basis of this example we see that May's horizontal leakage and the receiver separation effects are related through (16) and that vertical velocity corrections are also possible using noncollocated systems.

One disadvantage of using noncollocated systems appears in some calibration procedures. In section 2, we saw that a calibration procedure is needed to eliminate the phase difference among receiver lines. Some of these procedures use long-term atmospheric data and assume that the mean off-vertical atmospheric return is zero [*Röttger et al.*, 1990; *Thorsen et al.*, 1997]. However, in the lower atmosphere, such a procedure will calibrate out the geometrical term (Γ) that is needed for vertical velocity corrections.

Following our analysis, the unambiguous determination of the off-vertical atmospheric returns requires

accurate measurements of the scattering parameters, i.e., ξ_h^2 when horizontal isotropic scattering is assumed or ξ_x^2, ξ_y^2 and ψ (orientation) for horizontal anisotropic scattering. The latter parameters can be obtained from a FCA procedure. This requirement is true not only for noncollocated SA systems but also for those that are collocated. On the other hand, vertical velocity corrections can be done without knowing the scattering parameters under both collocated and noncollocated SA systems.

4. Experimental Results

We have used the large VHF radar at the Jicamarca Radio observatory in Perú for our AOA studies. The Jicamarca radar operates at ~50 MHz ($\lambda \approx$ 6 m) and has an ~300 by 300 m antenna array. The antenna is composed of 64 separate modules. Each module consists of a 12 by 12 array of cross-polarized half-wave dipoles. In Figure 2, we show the antenna configuration for these experiments. For transmission, we phased four modules (section D) to point precisely vertically, with a one-way half-power beam width (HPBW) of ~4°. Antenna sections A, B, and C were used for reception. Each receiving antenna was pointed on axis (~−1.46° from vertical along the y axis, i.e., toward the SW) and had a one-way HPBW of ~8.2°. The outputs from each antenna were received, sampled, and recorded independently. Ground clutter effects in each receiver were reduced separately in both the real and imaginary signal channels from the recorded data. To do this, we calculated the mean complex voltages in each of the individual time blocks defined by the incoherent averaging period. We then fitted a second-degree polynomial to the time series of the real and imaginary components of these mean values. Ground

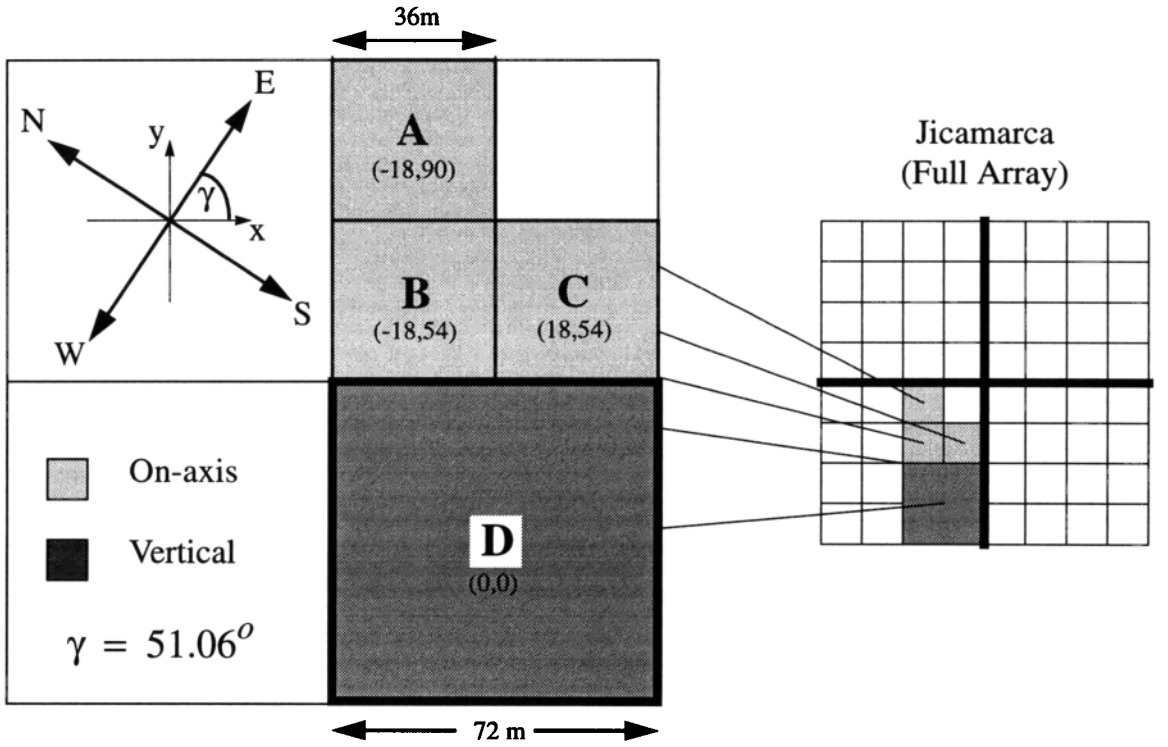

Figure 2. Antenna setup for the Jicamarca experiment. The transmitting antenna is the vertically pointing D module, and the receiving antennas are the "on-axis" pointing A, B, and C modules. The on-axis position differs from the zenith position because the antenna surface is not exactly horizontal but is tilted ~1.46°, approximately toward the southwest. Notice that neither of the antenna axes (x, y), is aligned with the geographic coordinates (E,N). The antenna centers are given in (x, y) coordinates with respect to the transmitting antenna center.

Table 1. Operating Parameters for the Experiments Conducted at Jicamarca During March 25-29, 1997

Parameter	Value
Pulse repetition period	2 ms
Number of coherent integrations	128
Number of incoherent integrations	6
Number of points	128
Effective sampling time	256 ms
Transmitter pulse width	3 μs
Receiver bandwidth	3 μs
Height resolution	0.45 km
Initial height	3 km
Number of heights	40
Transmitting power	100 kW

clutter effects were removed by subtracting this function from the original voltages values to provide the modified time series for subsequent analysis.

We present here the results of a 5-day run taken in March 1997 (from March 25, 1650 LT to March 29, 2215 LT). The operational parameters for this data set are presented in Table 1.

A calibration procedure was performed before and after the experiment to determine the possible phase differences arising from differing lengths of the receiving lines. Briefly, a common signal (either an output from one of the antennas or amplified sky noise) was fed in parallel to each of the receiving lines (cables, front-ends, amplifiers, and receivers). This signal was recorded and processed using parameters similar to those listed in Table 1. Phase differences determined from this process were incorporated into the subsequent analysis.

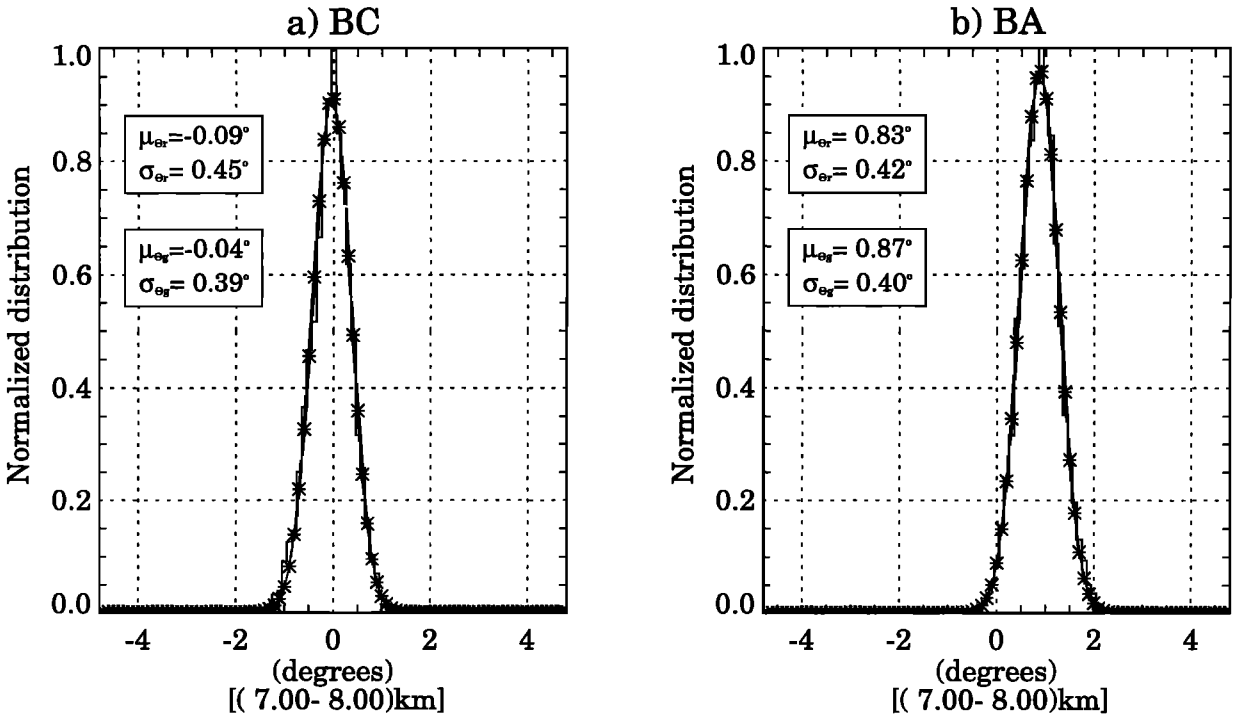

Figure 3. Histograms of 3-min angles of arrival (AOAs) obtained by a time domain method (see section 2.2) using the BC (Θ_x), and BA (Θ_y) antenna pairs. Solid lines represent the actual measurements, and the fitted Gaussian functions are represented by asterisks. Mean (μ_Θ) and standard deviation (σ_Θ) of the AOA measurements are given for the "raw" (subscript r) and Gaussian fitted (subscript g) data. These AOA measurements are relative to the plane of receiving antennas (see Figure 2) and include heights between 7 and 8 km.

AOA measurements were obtained every ~3 min using both time and frequency domain methods (see section 2.2). In both methods the measured AOA includes the four contributions described in section 2.1. We have ignored estimates with very low signal-to-noise ratio (SNR < -6 dB, after coherent integration) in our analysis. It is important to point out that the AOAs presented next are relative to the antenna surface and not to the horizontal plane (see Figure 2 for details).

We determined the time domain AOAs by fitting a straight line to the phase of each CCF pair (BA, BC, and CA) and evaluating that line at $\tau = 0$. This process was used in order to minimize the residual contributions from noise at $\tau = 0$.

In Figure 3, we present histograms of AOAs obtained in this manner in the two orthogonal bases BC and BA (see Figure 2) for heights between 7 and 8 km. This figure shows the distributions of "raw" AOA values (solid line) and a Gaussian-fitted function (asterisks). Mean (μ_Θ) and standard deviation (σ_Θ) values are shown for both the raw (subscript r) and Gaussian-fitted (subscript g) data. Note that the results are almost the same with and without Gaussian fitting. As mentioned above, these AOA values are relative to the plane of the receiving antennas, i.e., the true zenith position translates into $\Theta_{BC} = 0°$ and $\Theta_{BA} = 1.46°$.

In Figure 4, we present results for the frequency domain AOAs in a format similar to Figure 3 for the same time period. We obtained these measurements by fitting a line to the phase of the CSFs and evaluating them at $f = f_d$, where f_d is the Doppler shift of the respective CSF (see section 2.2). Examination of this figure shows the presence of more outliers in the frequency domain results than when using the time domain method. The outliers are graphically manifested by the presence of a constant "floor" ex-

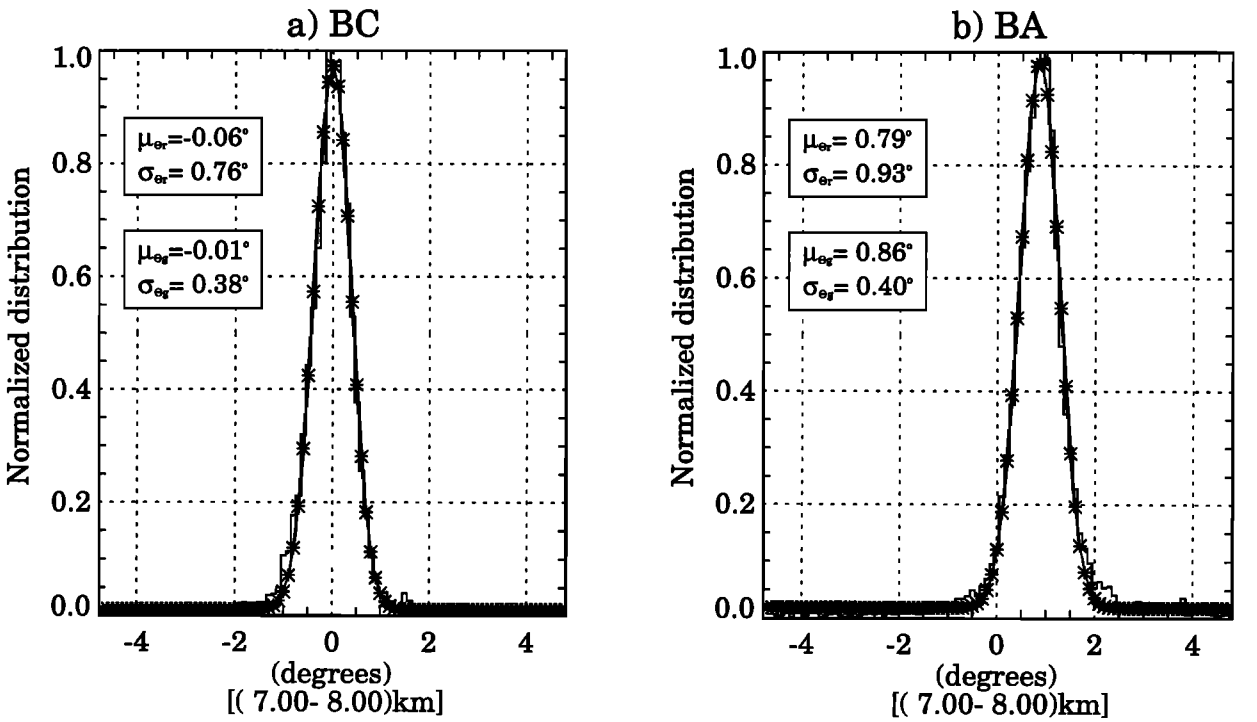

Figure 4. Histograms of 3-min AOAs obtained by a frequency domain method (see section 2.2) using the BC (Θ_x), and BA (Θ_y) antenna pairs. Solid lines represent the actual measurements, and the fitted Gaussian functions are represented by asterisks. Mean (μ_Θ) and standard deviation (σ_Θ) of the AOA measurements are given for the raw (subscript r) and Gaussian fitted (subscript g) data. These AOA measurements are relative to the plane of receiving antennas (see Figure 2) and include heights between 7-8 km.

tending across the histograms, i.e., values that raise the level of the base of the Gaussian-like functions at all values of AOAs. These outliers are also noticed in the standard deviation values, where $\sigma_{\Theta r}$ is considerably larger than $\sigma_{\Theta g}$ for both baselines. Note that the Gaussian fitted values are similar to those obtained from the time domain measurements.

From these similarities, we see that both methods give essentially the same information. It is important to point out that implementation is easier and calculation is faster in the time domain. Frequency domain methods, however, have the distinct advantage when interference is encountered. In the following analysis, we will use only AOAs obtained with the time domain method.

We now compared results obtained using the expressions presented in section 2.1 with those obtained from measured values of AOAs. The (x, y) receiver locations relative to the transmitter are $\boldsymbol{\rho}_A = (-18\text{ m}, 90\text{ m})$, $\boldsymbol{\rho}_B = (-18\text{ m}, 54\text{ m})$ and $\boldsymbol{\rho}_C = (18\text{ m}, 54\text{ m})$ (see Figure 2). The transmitting beam position is $\boldsymbol{\theta}_0 = (0, 1.46°)$ where 1.46° is the tilt of the antenna plane. The beam widths $\sigma_{T,R}$ (in meters) are related to the $\text{HPBW}_{T,R}$ (in radians) by $\sigma_{T,R} = z_0 \text{HPBW}_{T,R}/(2\sqrt{2\ln 2})$. Using these values, we have calculated the theoretical AOAs assuming an isotropic atmosphere ($\rho_{ch} \ll a_h^{-1}$). These theoretical curves are shown in Figure 5 for the two orthogonal baselines. The transmitting beam contribution ($2\Psi\xi_h^{-2}$) is shown by asterisks, the variable geometrical contribution ($2\Gamma\xi_h^{-2}$) is shown by plus signs, the constant geometrical contribution (Λ) is shown by diamonds, and the combined contribution $[2(\Psi+\Gamma)\xi_h^{-2}+\Lambda]$ is shown by triangles. Notice the constant value of zero, for all contributions, in baseline BC (aligned with x). These values will be the same if the isotropic condition is not satisfied ($\xi_h^2 \neq 2a_h^{-2}$). This result is mainly due to symmetric locations (in x) of receiving antennas B and C with respect to the transmitting antenna (see Figure 2).

For baseline BA the combined contributions have an asymptotic behavior with height, toward the antenna pointing contribution ($2\Psi\xi_h^{-2}$). If the atmosphere is specular ($\xi_h^2 \to \infty$), extreme case, the com-

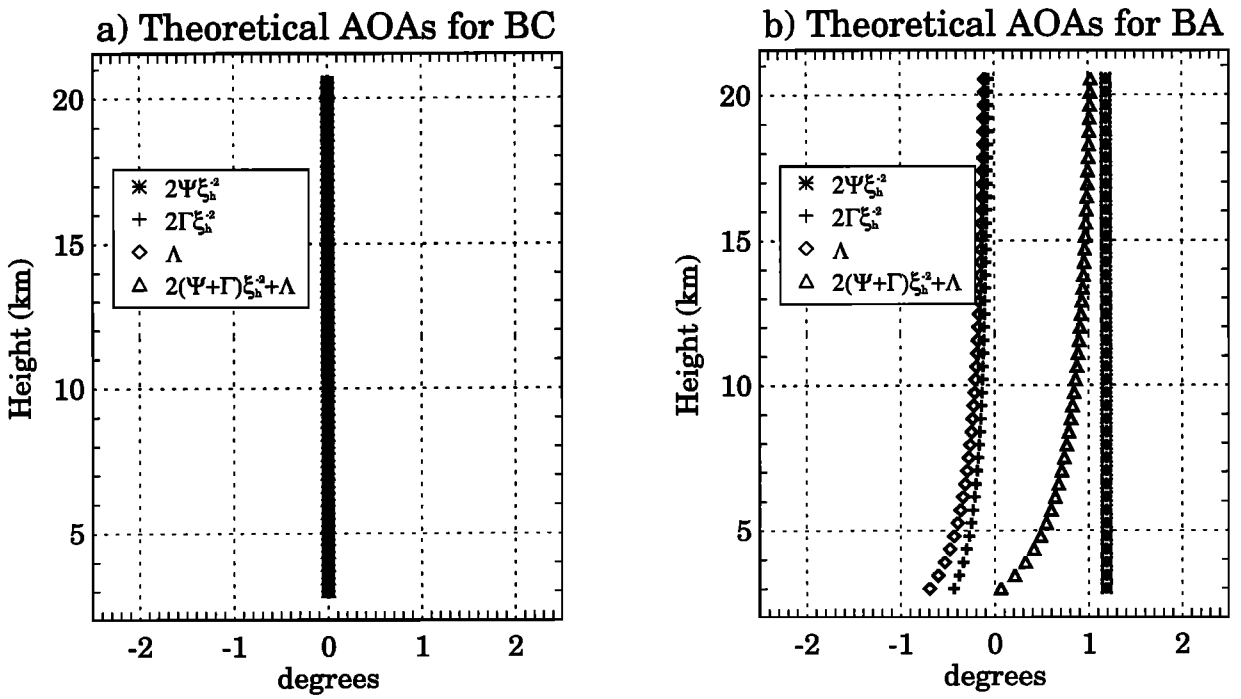

Figure 5. Theoretical AOAs under isotropic conditions ($\xi_h^2 \approx 2a_h^{-2}$), including just the spaced antenna (SA) system contributions: transmitting beam contribution ($2\Psi\xi_h^{-2}$), two geometric terms ($2\Gamma\xi_h^{-2}$ and Λ), and the combined contribution $[2(\Psi+\Gamma)\xi_h^{-2}+\Lambda]$. (a) BC ($\Theta_x$), and (b) BA ($\Theta_y$).

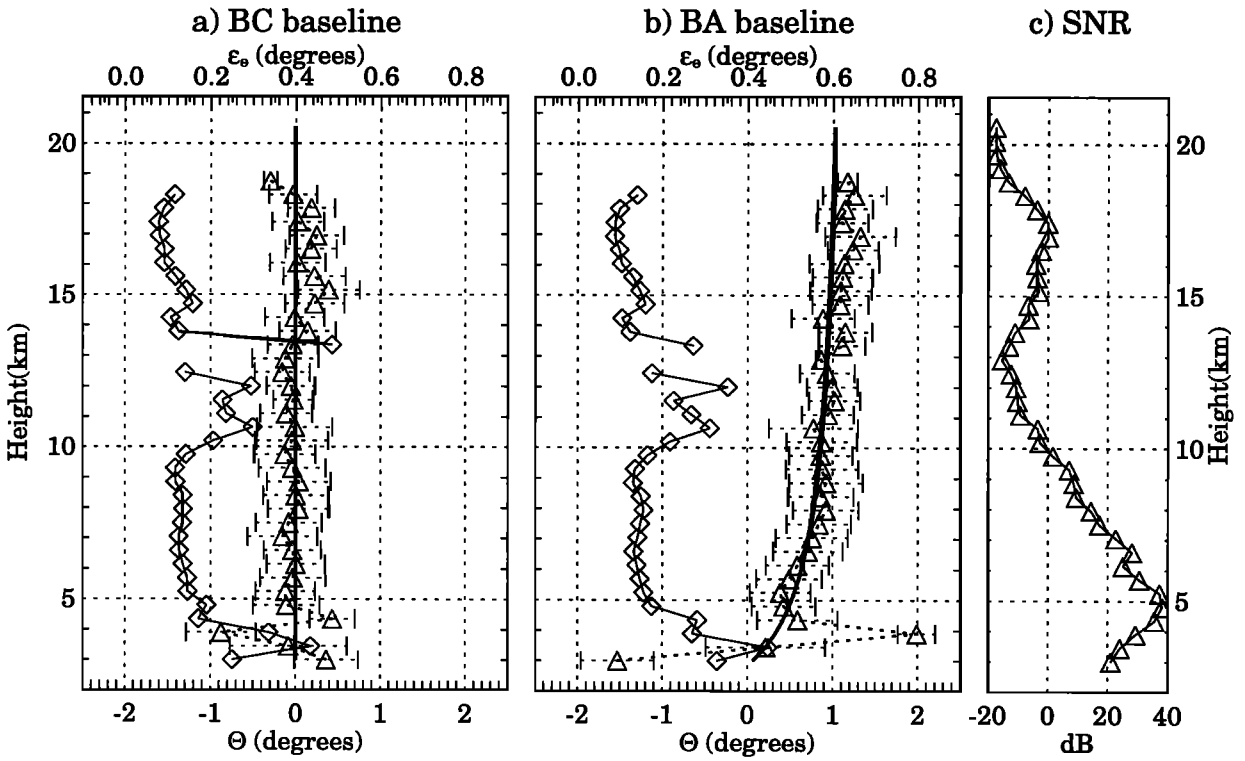

Figure 6. AOA profiles for the 5-day data set. AOA results for (a) baseline BC (Θ_x) and (b) baseline BA (Θ_y). The mean signal-to-noise ratio (SNR) profile appears in Figure 6c. The means and standard deviations of empirical values (triangles and horizontal dotted lines, respectively), are shown in Figures 6a and 6b using the bottom scales, along with the mean theoretical value for isotropic conditions (bold solid line). Statistical errors (ε_Θ), denoted by diamonds, are shown in Figures 6a and 6b plotted using the top scales.

bined contribution will be just the constant geometrical term (Λ). Moreover, Λ decreases with increasing height.

In Figures 6a and 6b, we present the 5-day AOA measurements for both orthogonal baselines (BC and BA), and in Figure 6c we show the mean SNR profile. The mean AOAs (triangles) are compared with the theoretical AOAs assuming isotropic conditions (bold line, $[2(\Psi+\Gamma)\xi_h^{-2}+\Lambda]$ shown in Figure 5). Sampled standard deviations are denoted with horizontal dashed lines. On the upper axis, we present the median value of the statistical errors of the AOAs ε_Θ (diamonds, see equation (28)), with values <0.2° for heights with good SNR. Notice the excellent agreement between the empirical and theoretical mean values, particularly in the lower heights (<15 km). The small differences in the near-tropopause heights (~17 km) could arise from nonisotropic scattering and/or "off-vertical" atmospheric returns [$\delta_0 \neq (0,0)$] under anisotropic scattering.

We have tried to quantify the accuracy of (28) for the statistical errors of AOA measurements. In Figure 7, we have plotted both autocorrelation values of AOAs along with AOA time series for an 8-hour interval. The 3-min AOA values are represented by asterisks, and the 15-min smoothed values are represented by bold solid lines. The empirical statistical errors ($\hat{\varepsilon}_\Theta$) are shown by the arrows between the two horizontal lines in Figures 7a and 7c. These empirical values are obtained from the difference between the 3-min autocorrelation values and the autocorrelation of the smoothed values at $\tau = 0$. The theoretical statistical error (ε_Θ) is obtained using (28). Comparing these two values, we see that the theoretical value underestimates the empirical value for both baselines (in this example by ~35%). This un-

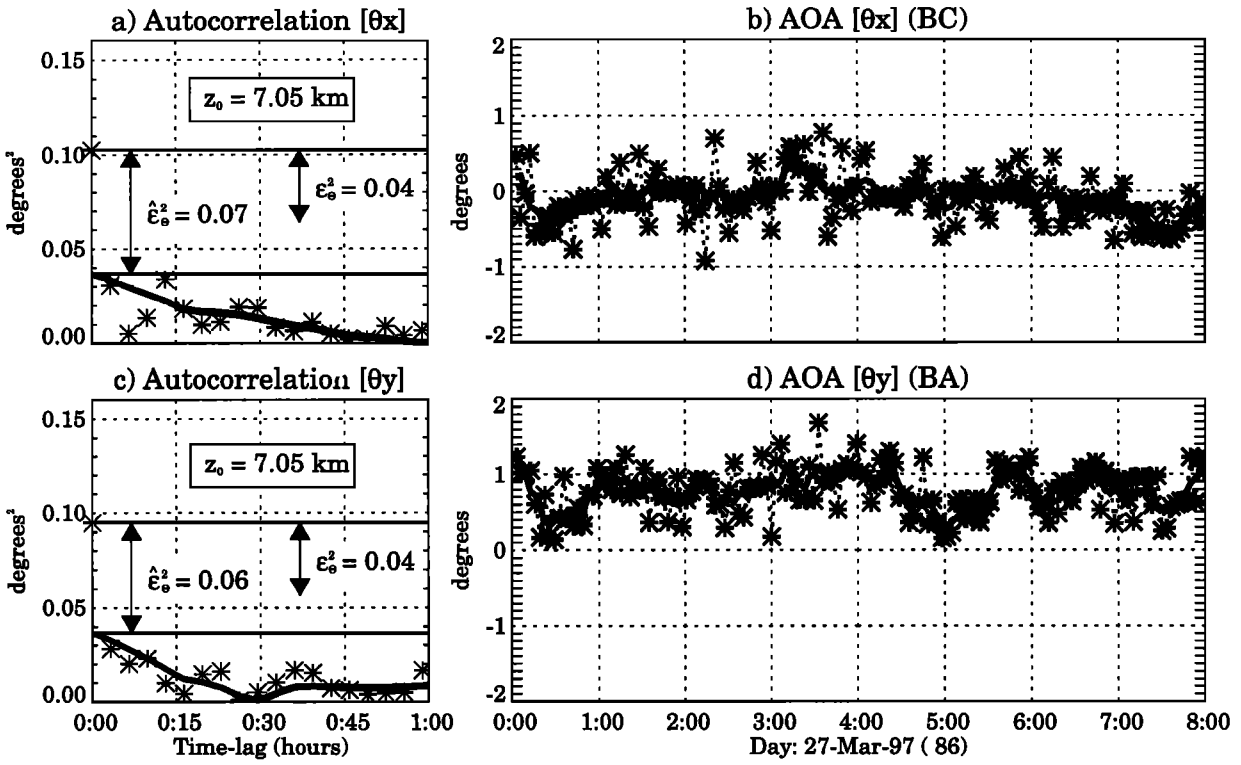

Figure 7. Examples of (a and c) AOA autocorrelation functions and (b and d) AOA time-series for baselines BC (Θ_x), and BA (Θ_y), respectively. AOA values for the 3-min measurements are represented in Figures 7b and 7d by asterisks. Corresponding 15-min smoothed curves are shown by a bold solid line. The empirical statistical variances are denoted by $\hat{\varepsilon}^2_\Theta$ (the horizontal lines in Figures 7a and 7c), and the theoretical value is denoted by ε^2_Θ (see equation (28)). The empirical values are obtained from the difference between the autocorrelation of the 3-min time series and the autocorrelation of the smoothed time series, at $\tau = 0$.

derestimation could be due either to the geophysical variability of the AOAs (notice the short-period oscillations in Figures 7b and 7d, with amplitudes <0.5°) or to inherent limitations involved in the approximations used in deriving (28).

The theoretical and empirical statistical errors translate into CCF phase errors of $\varepsilon_\phi = 7.5°$ and $\hat{\varepsilon}_\phi \approx 9.6°$, respectively. The empirical values are closer to the model results presented by *Hocking et al.* [1989] (between 8° and 11° for similar coherence and time correlation values). This result, along with the fact that both statistical errors decrease in the same proportion if we use a larger number of points ($M > 768$ in (28)), results not presented here, suggest that underestimation errors indeed arise from limitations in (28). It is possible that a constant of proportionality could be obtained from model simulations like those presented by *May* [1988].

In Figure 8 we show histograms of correlation times τ_c (Figure 8a), obtained from the width of the average autocorrelation function. The coherence values, coh_{BC} and coh_{BA}, for the two orthogonal baselines are shown in Figures 8b and 8c. The mean values in all panels are represented by dashed vertical lines, and theoretical values under isotropic conditions are represented by solid vertical lines. Any differences between these two values are presumably due to anisotropic scattering, i.e., $\xi_h^2 \neq 2a_h^{-2}$.

In Figure 9, we show an ~3-day data set of 3-min AOAs for six separate heights. The theoretical "isotropic" mean values for both baselines, BC and BA, are represented by long dashed horizontal lines. Short-dashed lines (in Figure 9b) show the zero values at each height (recall the nonzero value of the BA AOAs, due to the geometry and antenna pointing). Examination of Figure 9 shows the pres-

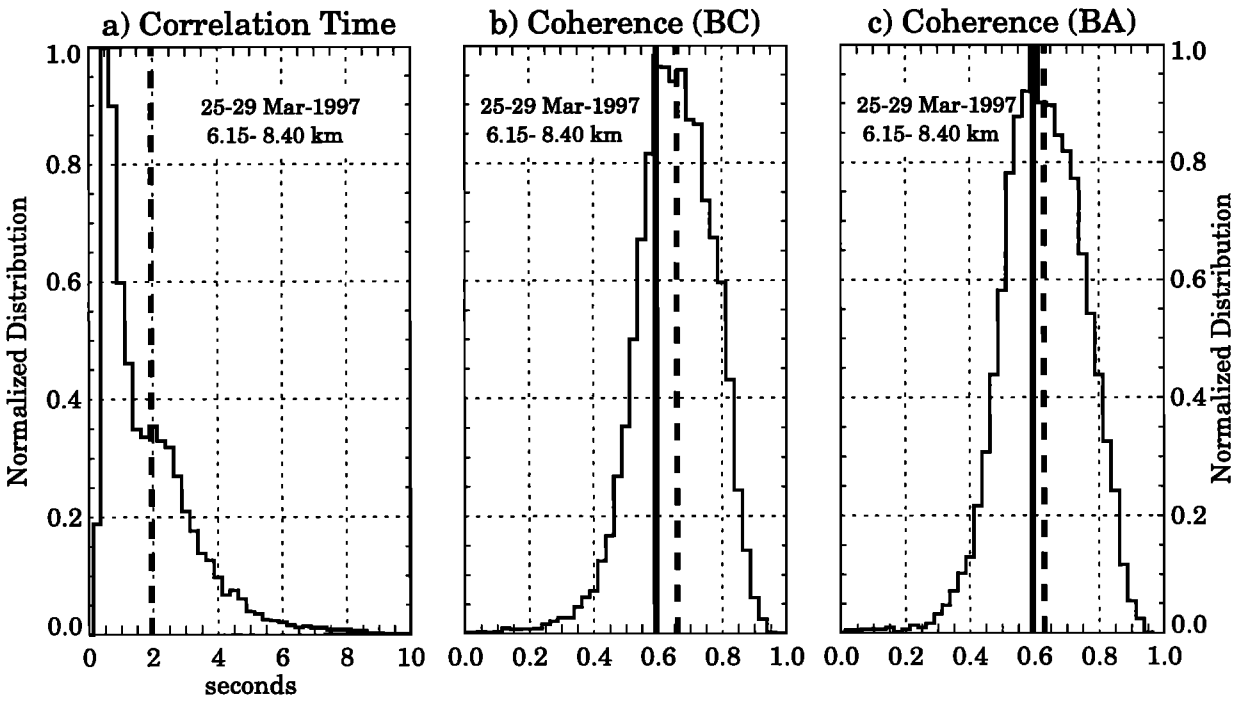

Figure 8. Histograms of (a) correlation times (τ_c) and coherence for baselines (b) BC ($\mathrm{coh_{BC}}[0]$) and (c) BA ($\mathrm{coh_{BA}}[0]$). The mean values in all panels are represented with vertical dashed lines, and the theoretical values under isotropic conditions ($\xi_h^2 \approx 2a_h^{-2}$) (Figures 8b and 8c) are represented by vertical solid lines. The analysis is done for heights between 6.15 and 8.40 km.

ence of long-period wave-like oscillations (>12 hours) with amplitudes of ~1° (with respect to the theoretical mean values). These oscillations, which exhibit some coherency with height, are related clearly to geophysical causes. *Röttger et al.* [1990] also related the AOA periodicities to long-period waves, with amplitudes of 1°-2°. *Palmer et al.* [1998] and *Tsuda et al.* [1997a] have both observed wave-like structure in the azimuth scans of echo power and relate them to gravity wave effects. These types of AOA oscillations have also been seen in the mesosphere by *Meek and Manson* [1992], using MF radar and attributed by them to gravity waves.

5. Conclusions

On the basis of scattering theory, we have identified four separate contributions to AOA lower-atmospheric VHF radar measurements. Specifically, we can isolate contributions from (1) tilted layers, (2) antenna pointing, and (3) two additional geometrical contributions, one dependent on the horizontal correlation length of the scatterers and one independent of such correlation length. We have also shown that the estimation of most AOA contributions requires the measurement of the scattering parameters, under both horizontally isotropic (ξ_h^2) and horizontally anisotropic (ξ_x^2, ξ_y^2, ψ) scattering. Therefore we recommend to use SA systems instead of conventional five-beam DBS systems when the measurements of AOAs and scattering parameters are needed.

On the basis of our theoretical derivation, it appears possible to relate AOA measurements to vertical wind velocities (see equation (19)). The correction of vertical velocities can be done without explicitly determining most AOA contributions (e.g., the tilt of reflecting structures).

Measurements of AOAs by noncollocated SA systems have been analyzed and discussed. We have shown that in theory, vertical velocity corrections can be done with such SA systems. The unambiguous determination of the tilt of reflecting structures depends on the precision of (1) the SA system (e.g., beam pointing, antenna positions) and (2) the mea-

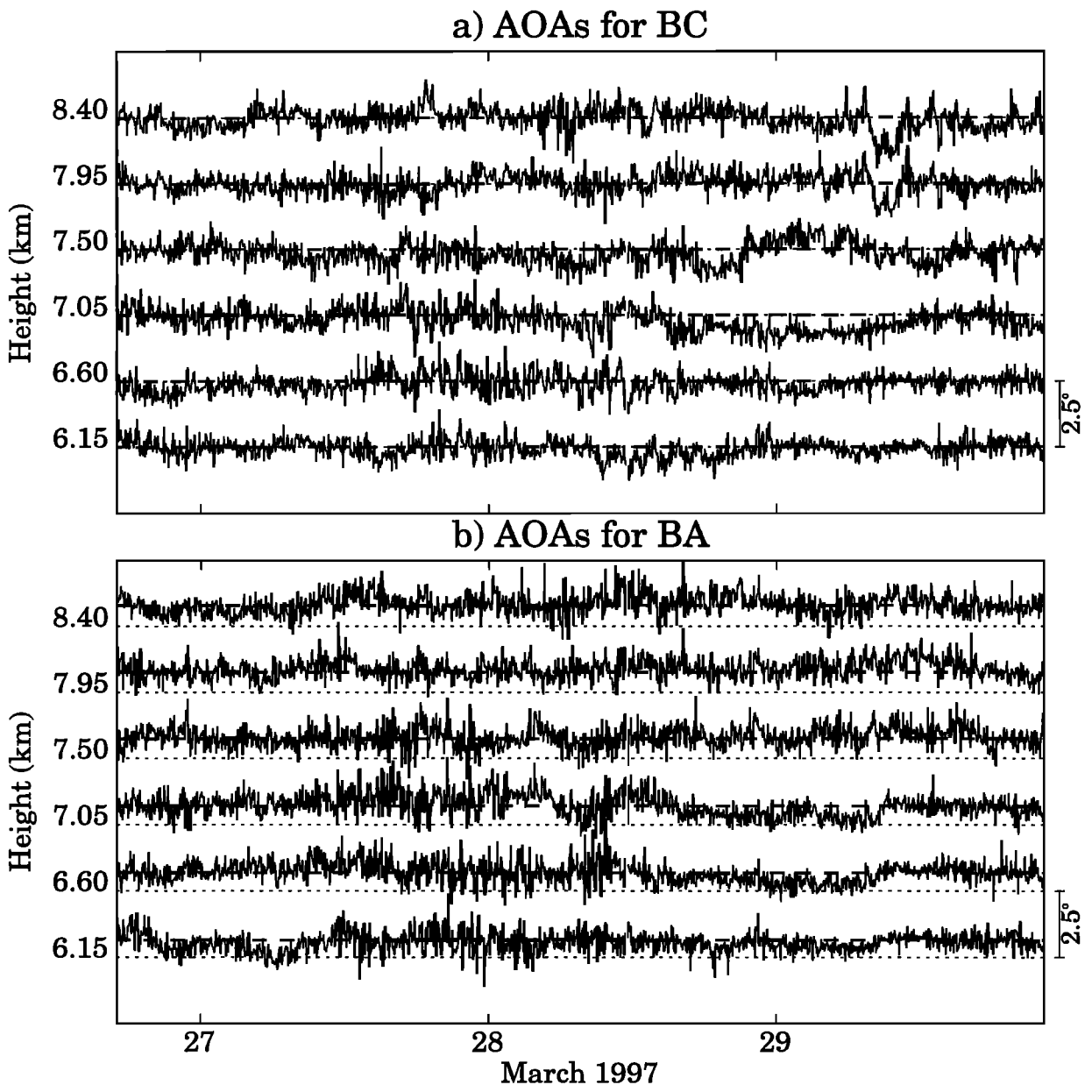

Figure 9. Time series of 3-min AOAs for six tropospheric heights (6.15 to 8.40 km). Results for baselines (a) BC (Θ_x), and (b) BA (Θ_y). Mean theoretical values under isotropic conditions ($\xi_h^2 \approx 2a_h^{-2}$) are represented by long-dashed lines. The short-dashed lines in Figure 9b represent the zero values at each height. Notice the long-period oscillations (>12 hours).

surement of scattering parameters. Nonetheless, this is also the case for collocated SA systems. The experimental corrections of vertical velocities are currently under study and will be presented in a future work.

We have compared frequency domain AOA estimates to those from the time domain method. Both methods give essentially the same information. However, the frequency domain AOA estimates exhibited more variance (more outliers) in our implementation, and their accuracy depends on the precision of the Doppler frequency measurement. In addition, the time domain method is easier to implement, faster

to calculate, and more reliable than the frequency domain method.

The nonatmospheric AOA contributions, assuming isotropic scattering ($\rho_{ch} \ll a_h^{-1}$), compared reasonably well with the experimental results, particularly below 15 km. Small differences above 15 km are probably due to anisotropic scattering and/or tilted layers.

Given the reasonable agreement between the empirical and theoretical statistical errors discussed here, a strong geophysical component can be seen in our AOA results. This geophysical component exhibit both short-period (<1 hour) and long-period (>12 hours) oscillations with ~1° amplitudes. The detailed characterization of these AOAs measurements and their relationship to gravity waves, vertical velocities, and aspect sensitivity will be left for future work.

One possible limitation to this derivation is that the time stationary wind component of the turbulent flow has been assumed spatially homogeneous. Recently, *Larsen and Palmer* [1997], *Palmer et al.* [1997], and *Pan et al.* [1996] have suggested that AOAs could be affected by wind field inhomogeneities. The implications of these inhomogeneities on the present development are also left for a future study.

Appendix: AOA Interpretation Under Horizontally Anisotropic Scattering

Using *Holloway et al.* [1997, equation (21)] and the AOA contributions of section 2.1, we arrive at the following normalized cross-correlation function:

$$c_{ij}(\tau) \approx \exp\left\{-\frac{2(v'_{0x}\tau - \Delta\rho'_{xij}/2)^2}{\xi_x^2} - \frac{2(v'_{0y}\tau - \Delta\rho'_{yij}/2)^2}{\xi_y^2} - 2(k_0\sigma_t\tau)^2 - \frac{1}{8}\left(\frac{v_{0z}\tau}{\sigma_r}\right)^2 + j\phi_{ij}(\tau)\right\} \quad \text{(A1)}$$

where

$$\begin{aligned}\phi_{ij}(\tau) \approx\ & -2k_0 v_{0z}\tau - 2k_0 v'_{0x}\Theta'_{xij}\tau \\ & -2k_0 v'_{0y}\Theta'_{yij}\tau + k_0\Delta\rho'_{xij}\Theta'_{xij} \\ & +k_0\Delta\rho'_{yij}\Theta'_{yij} + k_0|\Delta\rho'_{ij}|\Lambda_{ij} \quad \text{(A2)}\\ \Theta'_{xij} =\ & 2(\Omega'_x + \Phi'_x + \Gamma'_{xij})\xi_x^{-2} \\ \Theta'_{yij} =\ & 2(\Omega'_y + \Phi'_y + \Gamma'_{yij})\xi_y^{-2}\end{aligned}$$

$$\begin{aligned}\xi_x^2 &= 2a_h^{-2} + (2\rho'_{cx})^2 \\ \xi_y^2 &= 2a_h^{-2} + (2\rho'_{cy})^2\end{aligned}$$

and ρ'_{cx} and ρ'_{cy} are the correlation lengths along the primed coordinate axes (x', y').

The irregularities are assumed to have the major/minor axes of their correlation ellipse aligned along the $x' - y'$ axes, which are rotated by an unknown angle ψ with respect to the $x-y$ axes (the axes that define the transmitter and receiver locations).

Now the primed coordinate system $(x' - y')$ is related to the $x - y$ system by the following transformation:

$$\boldsymbol{X}' = \boldsymbol{T}\boldsymbol{X} \quad \text{(A3)}$$

where $\boldsymbol{X}' = (x', y')$, $\boldsymbol{X} = (x, y)$, and

$$\boldsymbol{T} = \begin{pmatrix} \cos\psi & \sin\psi \\ -\sin\psi & \cos\psi \end{pmatrix} \quad \text{(A4)}$$

Applying these transformations to all the primed variables (velocity, position, and AOA contributions), the phase term given by (A2) becomes

$$\begin{aligned}\phi_{ij}(\tau) \approx\ & -2k_0 v_{0z}\tau - 2k_0 v_{0x}\Theta^a_{xij}\tau \\ & -2k_0 v_{0y}\Theta^a_{yij}\tau + k_0\Delta\rho_{xij}\Theta^a_{xij} \\ & +k_0\Delta\rho_{yij}\Theta^a_{yij} + k_0|\Delta\rho_{ij}|\Lambda_{ij} \quad \text{(A5)}\end{aligned}$$

where $(\Theta^a_{xij}, \Theta^a_{yij})$ represents the observed AOA vector and is given by

$$\begin{aligned}\Theta^a_{xij} =\ & \Theta_{xij}(\cos^2\psi + (\xi_x^2/\xi_y^2)\sin^2\psi) \\ & +\Theta_{yij}\cos\psi\sin\psi(\xi_y^2/\xi_x^2 - 1) \quad \text{(A6)}\\ \Theta^a_{yij} =\ & \Theta_{yij}(\cos^2\psi + (\xi_y^2/\xi_x^2)\sin^2\psi) \\ & +\Theta_{xij}\cos\psi\sin\psi(1 - \xi_x^2/\xi_y^2) \quad \text{(A7)}\end{aligned}$$

and

$$\begin{aligned}\Theta_{xij} &= 2(\Omega_x + \Phi_x + \Gamma_{xij})\xi_x^{-2} \quad \text{(A8)}\\ \Theta_{yij} &= 2(\Omega_y + \Phi_y + \Gamma_{yij})\xi_y^{-2} \quad \text{(A9)}\end{aligned}$$

The influence of horizontal anisotropic irregularities on the statistical errors is mainly through the correlation time (τ_c) and through the coherence term ($\mathrm{coh}_{ij}[0]$). Transforming (A1) to the $x - y$ axes, the square of the coherence term becomes

$$\mathrm{coh}^2_{ij}[0] = \exp\left\{-\frac{\Delta\rho^2_{xij}(\xi_x^{-2}\cos^2\psi + \xi_y^{-2}\sin^2\psi)}{2} + \frac{\Delta\rho^2_{yij}(\xi_y^{-2}\cos^2\psi + \xi_x^{-2}\sin^2\psi)}{2} + \frac{\Delta\rho_{xij}\Delta\rho_{yij}\cos\psi\sin\psi(\xi_x^{-2} - \xi_y^{-2})}{2}\right\} \quad \text{(A10)}$$

Acknowledgments. The authors gratefully acknowledge helpful inputs from R. J. Doviak (NOAA - NSSL) that help to clarify important issues of this work. We also would like to thank D. Thorsen (University of Colorado), R. D. Palmer (University of Nebraska), and an anonymous reviewer for their comments and suggestions on the original manuscript. The help and dedication of the Jicamarca Radio Observatory staff (in particular, F. Villanueva) during the experiment are appreciated. This work has been supported by the National Science Foundation under grants ATM-9214657 and ATM-9614700.

References

Adams, G. W., J. W. Brosnahan, D. C. Walden, and S. F. Nerney, Mesospheric observations using a 2.66-MHz radar as an imaging Doppler interferometer: Description and first results, *J. Geophys. Res.*, *91*, 1671–1683, 1986.

Briggs, B. H., The analysis of spaced sensors records by correlation techniques, in *Handbook for the Middle Atmosphere Program*, pp. 166–186, SCOSTEP Secr., Univ. of Ill., Urbana, 1984.

Briggs, B. H., and R. A. Vincent, Spaced-antenna analysis in the frequency domain, *Radio Sci.*, *27*, 117–129, 1992.

Doviak, R. J., R. J. Lataitis, and C. L. Holloway, Cross correlations and cross spectra for spaced antenna wind profilers, *Radio Sci.*, *31*, 157–180, 1996.

Franke, P. M., D. Thorsen, M. Champion, S. J. Franke, and E. Kudeki, Comparison of time- and frequency-domain techniques for wind velocity estimation using multiple-receiver MF radar data, *Geophys. Res. Lett.*, *17*, 2193–2196, 1990.

Fukao, S., T. Sato, T. Tsuda, M. Yamamoto, M. D. Yamanaka, and S. Kato, MU radar: New capabilities and system calibrations, *Radio Sci.*, *25*, 477–485, 1990.

Green, J. L., and K. S. Gage, Observations of stable layers in the troposphere and stratosphere using VHF radar, *Radio Sci.*, *15*, 395–405, 1980.

Hocking, W. K., P. May, and J. Röttger, Interpretation, reliability and accuracies of parameters deduced by spaced antenna method in middle atmosphere applications, *Pure Appl. Geophys.*, *130*, 571–604, 1989.

Holdsworth, D. A., An investigation of biases in the full spectral analysis technique, *Radio Sci.*, *32*, 769–782, 1997.

Holdsworth, D. A., and I. M. Reid, A simple model of atmospheric radar backscatter: Description and application to the full correlation analysis of spaced antenna data, *Radio Sci.*, *30*, 1263–1280, 1995.

Holloway, C., R. Doviak, and S. Cohn, Cross correlations of fields scattered by horizontally anisotropic refractive index irregularities, *Radio Sci.*, *32*, 1911–1920, 1997.

Huaman, M. M., and B. Balsley, Long-term average vertical motions observed by VHF wind profilers: The effect of slight antenna-pointing inaccuracies, *J. Atmos. Oceanic Technol.*, *13*, 560–569, 1996.

Larsen, M. F., and R. D. Palmer, A relationship between horizontal flow gradients, in-beam incidence angles, and vertical velocities, *Radio Sci.*, *32*, 1269–1277, 1997.

Larsen, M. F., and J. Röttger, The spaced antenna technique for radar wind profiling, *J. Atmos. Oceanic Technol.*, *6*, 920–938, 1989.

Larsen, M. F., and J. Röttger, VHF radar measurements of in-beam incidence angles and associated vertical-beam radial velocity corrections, *J. Atmos. Oceanic Technol.*, *8*, 477–490, 1991.

Liu, C. H., J. Röttger, C. J. Pan, and S. J. Franke, A model for spaced antenna observational mode for MST radars, *Radio Sci.*, *25*, 551–563, 1990.

May, P. T., Statistical errors in the determination of wind velocities by the spaced antenna technique, *J. Atmos. Sol. Terr. Phys.*, *50*, 21–32, 1988.

May, P. T., Comments on "VHF radar measurements of in-beam incidence angles and associated vertical-beam radial velocity corrections", *J. Atmos. Oceanic Technol.*, *10*, 432–434, 1993.

Meek, C. E., An efficient method for analysing ionospheric drifts data, *J. Atmos. Sol. Terr. Phys.*, *42*, 835–839, 1980.

Meek, C. E., and A. H. Manson, Angle-off-arrival oscillations in the mesosphere as seen by medium frequency (MF) radar, *J. Atmos. Sol. Terr. Phys.*, *54*, 277–293, 1992.

Muschinski, A., Possible effect of Kelvin-Helmholtz instability on VHF radar observations of the mean vertical wind, *J. Appl. Meteorol.*, *35*, 2210–2217, 1996.

Palmer, R. D., M. F. Larsen, R. F. Woodman, S. Fukao, M. Yamamoto, T. Tsuda, and S. Kato, VHF radar interferometry measurements of vertical velocity and the effect of tilted refractivity surfaces on standard Doppler measurements, *Radio Sci.*, *26*, 417–427, 1991.

Palmer, R. D., K. Y. Lei, S. Fukao, M. Yamamoto, and T. Nakamura, Weighted imaging Doppler interferometry, *Radio Sci.*, *30*, 1787–1801, 1995.

Palmer, R. D., S. Vangal, M. F. Larsen, S. Fukao, T. Nakamura, and M. Yamamoto, Phase calibration of VHF spatial interferometry radars using stellar sources, *Radio Sci.*, *31*, 147–156, 1996.

Palmer, R. D., M. F. Larsen, and S. Vangal, Effects of finite beam width and wind field divergence on Doppler radar measurements: Simulations, *Radio Sci.*, *32*, 1179–1191, 1997.

Palmer, R. D., M. F. Larsen, S. Fukao, and M. Yamamoto, On the relationship between aspect sensitivity and spatial interferometric in-beam incidence angles, *J. Atmos. Sol. Terr. Phys.*, *60*, 37–48, 1998.

Pan, C. J., and C. H. Liu, A model for oblique spaced antenna techniques for mesosphere-stratosphere-troposphere radars and its applications, *Radio Sci.*, *27*, 131–144, 1992.

Pan, C. J., C. H. Liu, and J. Röttger, Effects of an inhomogeneous wind field on the spaced antenna method, in *Proceedings of the Seventh Workshop on Technical and Scientific Aspects of MST Radar*, pp. 396–398, SCOSTEP Secr., NOAA, Boulder, Colorado, 1996.

Röttger, J., and H. M. Ierkic, Postset beam steering and interferometer applications to VHF radars to study winds, waves, and turbulence in the lower and middle atmosphere, *Radio Sci.*, *20*, 1461–1480, 1985.

Röttger, J., and C. H. Liu, Partial reflection and scattering of VHF radar signals from the clear atmosphere, *Geophys. Res. Lett.*, *5*, 357–360, 1978.

Röttger, J., C. H. Liu, J. K. Chao, A. J. Chen, C. J. Pan, and I.-J. Fu, Spatial interferometer measurements with the Chung-Li VHF radar, *Radio Sci.*, *25*, 503–515, 1990.

Thorsen, D., A statistical climatology of mesospheric gravity wave activity over Urbana, Ph.D. thesis, Univ. of Ill., Urbana-Champaign, 1996.

Thorsen, D., S. J. Franke, and E. Kudeki, A new approach to MF radar interferometry for estimating mean winds and momentum flux, *Radio Sci.*, *32*, 707–726, 1997.

Tsuda, T., T. Sato, K. Hirose, S. Fukao, and S. Kato, MU radar observations of the aspect sensitivity of backscattered VHF echo power in the troposphere and lower stratosphere, *Radio Sci.*, *21*, 971–980, 1986.

Tsuda, T., W. E. Gordon, and H. Saito, Azimuth angle variations of specular reflection echoes in the lower atmosphere observed with the MU radar, *J. Atmos. Sol. Terr. Phys.*, *59*, 777–784, 1997a.

Tsuda, T., T. E. VanZandt, and H. Saito, Zenith-angle dependence of VHF specular reflection echoes in the lower atmosphere, *J. Atmos. Sol. Terr. Phys.*, *59*, 761–775, 1997b.

Van Baelen, J. S., A. D. Richmond, T. Tsuda, S. K. Avery, S. Kato, S. Fukao, and M. Yamamoto, Radar interferometry technique and anisotropy of the echo power distribution: First results, *Radio Sci.*, *26*, 1315–1326, 1991.

Vandepeer, B. G. W., and I. M. Reid, Some preliminary results obtained with a new Adelaide MF Doppler radar, *Radio Sci.*, *30*, 1191–1203, 1995.

Vincent, R. A., P. T. May, W. K. Hocking, W. G. Elford, B. H. Candy, and B. H. Briggs, First results with the Adelaide VHF radar: Spaced antenna studies of tropospheric winds, *J. Atmos. Sol. Terr. Phys.*, *49*, 353–366, 1987.

B. Balsley and J. Chau, CIRES Building 318, University of Colorado, Campus Box 216, Boulder, CO 80309. (e-mail: balsley@terra.colorado.edu; chau@sipan.colorado.edu)

(Received October 31, 1997; revised February 17, 1998; accepted March 5, 1998.)